Journal of Engineering and Applied Sciences 13 (Special Issue 14): 11091-11107, 2018
ISSN: 1816-949X

Performance Evaluation of OSTBC-MC-CDMA with 4-Antennas MIMO Over Rayleigh Flat Fading Channel

Nader Abdullah Khadam, Arash Ahmadi, Seyed Vahab Makki and Golamreza Karimi
Department of Electrical Engineering, College of Engineering, Razi University, Kermanshah, Iran

Abstract: This study evaluates the OFDM performance over a flat fading Ryleigh channel. The simulated system incorporates the benefits of the orthogonal space-time block code with the Multi-Carrier Code Division Multiple Access (MC-CDMA) to enhance the performance of the OFDM over the multi-path channels.The environment is assumed to be a moving transmitter with speeds 2, 45 and 100 km/h with outdoor Rayleigh flat fading channel. The system employs 4 antennas at the receiver end to mitigate the effect of multipath signal. The system's orthogonal frequencies are generated using Haar, Daubechies 4 (dB4) 4, Symlets 4 (Sym4), Cohen-Daubechies-Feauveau (CDF) 1.1 and 9.7 and B-spline 3 (Bs3). The number of used carriers is 128, 256, 512, 1024 and 2048 with subcarriers 64, 180, 360 and 720. The modulation is QPSK with cyclic prefix 1/16 and bandwidth of 20 MHz. The system's BER is compared with the traditional FFT system to highlight the enhancements of using Discrete Wavelet Packet Transform (DWPT) instead the FFT method. The PN-s sequence is generated using gold code. The proposed system shows significant improvement in BER over the system that uses FFT to generate the orthogonal carriers and presents itself as a powerful candidate to replace these traditional FFT systems. The STBC is used as an enhancement to improve the system capability to correct the potentially erroneous bits within the frame due to the AWGN and channel Inter-Symbol Interference (ISI) in the channel. The results shows a significant improvement in the BER using this proposed arrangement.

Key words: Block code, DWPT, OFDM, CDMA, fading channels, data networks

INTRODUCTION

The modern society is currently measured by the amount of the data exchanged over the network channels. The network users were counted in a few thousands to several hundreds of thousands during the 80's. After the second millennium, the users grew exponentially to billions and each individual is using multiple devices at the same time. This explosion in the number of users flooded the communication channels with unprecedented data flow. The recent advancements in data network gave rise to many applications that are involved with almost every aspect of life ranging from top-secret military operation to merely sending greetings for a birthday (Moskvitch, 2017; Sewwandi *et al*., 2017; Xu *et al*., 2017). These data networks are widely spread over the world and continue to evolve as new subscribers are joining this new tide of information revolution.

These networks are becoming the backbone of societies because people are relying on them to spread news all over the world (Khan and Hoque, 2017; Mawele and Pellissier, 2016; Kaur and Garg, 2015, Zhang *et al*., 2015; Yamakami, 2017). Others are using them as a virtual market to advertise and sell their goods. Even the elections consider social networks as a reliable source of information to study the citizen's point of views regarding a certain party or a candidate (Pouryazdan *et al*., 2017; Sultana *et al*., 2017; Shi *et al*., 2017a, b). Decades ago, the users of these networks were satisfied with low level of quality service such as sending text messages that requires low bandwidth to deliver. Recently, the demands are increasing with the increase of social awareness and intelligence. The individuals now want to exchange High Definition Videos (HDTV), televised meetings across continents and video calls. This tremendous expansion demands a wide channel spectrum to transfer such barrage of data.

Presently, these networks are growing to be self-sustained economic systems and a pillar of modern societies. Therefore, their demands should be met as soon and as much as possible (Wicha *et al*., 2017; Chen *et al*., 2017; Kaur *et al*., 2017; Faisal *et al*., 2017; Samaraweera *et al*., 2017; Zhang *et al*., 2017). To satisfy the networks insatiable appetite for higher bandwidths, the engineers could follow the traditional way by providing the extra bandwidths for the networks. Due to

Corresponding Author: Nader Abdullah Khadam, Department of Electrical Engineering, College of Engineering, Razi University, Kermanshah, Iran

the fact that the resultant substreams have low rate and hence, low bandwidth requirements then the OFDM requires less channel compared with the classical system. The fact that the subcarriers are orthogonal also allows that the channels can overlap without interference because the orthogonality ensures complete separation among channels and hence, no carrier interference. Thus, this represents another reduction in the required channel bandwidth that cannot be afforded using the non-ortho

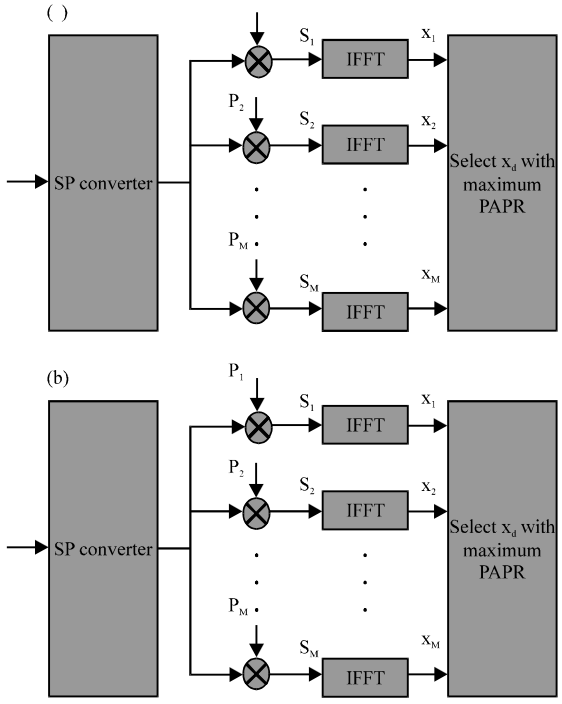

Fig. 1: OFDM block diagram; a) The transmitter and b) The receiver

gonal transmission (Schulze and Luders, 2005; Bahai and Saltzberg, 2002). The carriers and channels illustration is shown in Fig. 1 and 2. Although, this might be satisfactory but this approach is threatened by unavoidable limitations. First limitation is the scares affordable free bandwidth because the RF spectrum is highly congested. The second limitation is even if the bandwidth is available but stretching the bandwidth over a wide range increases the influence of nonlinearity and deformations effect on the transmitted signals. The third limitation is the short distance. When the users are now located at near distance transmitting high bitrates this leads to interference and accumulated error rates due to multipath signals. There are techniques that might combat these unwanted effects but still they need huge processing time which leads to accumulated delays.

To prevent the network from falling to the vice of the above limitations, the engineers invented an ingenious approach to modulate the data using narrower bandwidth with higher data rates. The new technique is called the Multi-Carrier transmission (MC) or its modern version the Orthogonal Frequency Division Multiplexing (OFDM).

Multi Carrier (MC) or Orthogonal Frequency Division Multiplexing (OFDM) system: The idea of OFDM is based on sub-dividing the high bit rate serial stream of data into a lower bit rate parallel stream segments. These segments are then modulated using orthogonal subcarriers to ensure neither overlapping between adjacent channels norco-channel interference among neighboring sub-channels. These sub-streams are combined together and transmitted usinga main

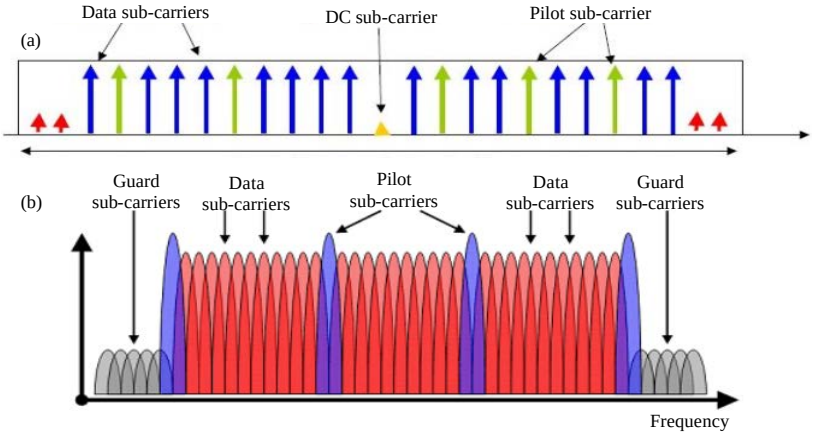

Fig. 2a): The subcarriers assignment to users with pilot carriers and b) OFDM signal spectrum

carrier before transmission. The block diagram of typical OFDM system is shown in Fig. 1. Figure 2b shows that even if the transmitted data are exposed to nonlinearity or bust noise then only a small percentage will be affected rather than the whole stream due to the fragmentation of the original data stream.

The main operation to generate an OFDM signal is the generation of the orthogonal carriers. This operation should be precise and accurate to ensure maximum data density otherwise the subcahnnels will tend to overlap and the system performance will degrade. There are methods to generate the orthogonal subcarriers but in this study only the Fast Fourier Transform (FFT) and the Discrete Wavelet Packet Transform (DWPT) will be considered.

MATERIALS AND METHODS

Orthogonal subcarriers generation using Inverse Fast Fourier Transform (IFFT): Consider a Multi-Carrier (MC) OFDM system with N subcarriers and each subcarrier f_k is used to modulate s_k sub-frame then the transmitted signal s(t):

$$s(t) = \sum_{k=1}^{N} s_k \exp(j2\pi k f_k t) \quad (1)$$

where, f_k is equally spaced subcarriers and f_k = BW/N. Let T to be 2/BW then according to Nyquist theorem each sample occurs at T/2 or 1/BW. Therefore, any sub-stream subcarrier at an instancewill exist at time mT then Eq. 1 becomes:

$$s(mT) = \sum_{k=1}^{N} s_k \exp\left(j2\pi \frac{km}{N}\right) \quad (2)$$

Equation 2 is exactly the Inverse Discrete Fourier Transform (IDFT) or its equivalent Inverse Fast Fourier Transform (IFFT) used by computing machines.

Equation 2 solves the complexity of generating N subcarriers, especially, when N is very large and they all should be at the precise period to ensure orthogonality. Hence, by taking the IFFT of the modulated signal it can be ensured that the sub-carries are accurately generated from only one input. At the receiver, an FFT circuit can be used to retrieve the transmitted signals from the incoming samples. This is quite clear from Fig. 1 where the symbols are modulated, possibly using QAM (Ramjee, 2004), after adding the correction codes if needed, then converted to lower bit rate using serial to parallelbefore the IFFT takes action. After generating the orthogonal subcarriers, the symbols are then recombined using parallel to serial circuit before transmission. At the receiver, the operations are reverse in order to acquire the source information. Figure 2a shows the orthogonal subcarriers generated using the IFFT while Fig. 2b shows how these subcarriers are used to modulatethe subframes s_k at the output of the parallel to serial.

Discrete Wavelet Packet Transform (DWPT): Equation 2 can be viewed as a running filter with coefficients exp (j2π km/N) or in other words a low pass filter bank. The frequency location for each subcarrier f_k occurs at every $2^k \times f_0$ where f_0 is the fundamental frequency and f_k are its harmonics. This means that the Power Spectral Density (PSD) will be widely spread over the channel as the sinusoidal function extends from -∞ to +∞. This consequently reduces the system spectral efficiency.

In order to solve this problem, the analyzing function exp (j2π km/N) can be replaced by a more compact or spectral efficient function to ensure higher PSD concentration (Khan *et al*., 2016). The Discrete Wavelet Transform DWT can ensure the achievement of this goal. Hence, by replacing DFT (or FFT) with DWT, the spectral efficiency can be increased due to time limited period of DWT functions resulting in a more reliable and higher signal quality (Soni *et al*., 2013; Roy *et al*., 2012; Bodhe *et al*., 2012a, b). The wavelets are orthonormal functions such that:

$$\langle \Psi_l(t), \Psi_k(t) \rangle = \int \Psi_l(t)\Psi_k(t)dt = \begin{cases} 1 & l=k \\ 0 & l\neq k \end{cases} \quad (3)$$

Where:

$\Psi(t)$ = The mother wavelet
$\langle . \rangle$ = Inner product

The wavelet functions should meet certain features such as the area under the curve should always equal to zero or the negative area equals the positive area. This feature ensures equal energy distribution. The second feature is that every wavelet function should have a limited number of vanishing moments (Olkkonen, 2011; Wickerhauser, 1994). The vanishing moments for $\Psi(t)$ can be found as:

$$\int_{-\infty}^{\infty} t^k \Psi(t)dt = 0 \quad \text{for } 0 \le k < p \quad (4)$$

The vanishing moments describe the speed of decay of the wavelet function. For any function x(t) the output of the analyzing DWT is:

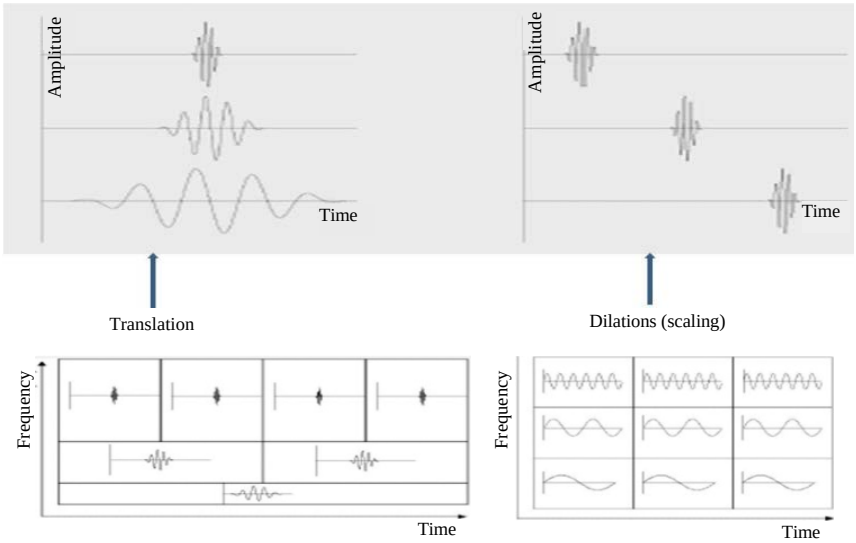

Fig. 3: The scale and translation of wavelet

$$X_{\Psi}(s,r)=\int_{-\infty}^{\infty} x(t)\Psi_{s,r}(t)\,dt \tag{5}$$

where, s, r are the scale and translation. This means that the wavelet can capture the details of x(t) in both time and frequency unlike FFT which focuses only on the frequency domain. The translation means the wavelet is shifted in time while the scale is related to the width of the finite wavelet function. The larger the scale in time the lower frequency components it can capture. The scale and translation are shown in Fig. 3 (Debnath and Shah, 2015). Assume an M samples discrete signal x[n] and n = 0, 1, ... , M-1. Applying the first level DWT to x(n) then:

$$y[n]=\sum_{k=-\infty}^{\infty} x[k]G_0[2n-k]+\sum_{k=-\infty}^{\infty} x[k]G_1[2n-k]= y_{low}[n]+y_{high}[n] \tag{6}$$

Equation 6, the y_{low} is the signal coming from the LPF bank with its impulse response $G_0[2n-k]$ while y_{high} is the signal coming from the HPF bank with its impulse response $G_1[2n-k]$. It is noted that the out coming signal has double the sampling rate n as the input signal. Thus, a decimation circuit by 2(↓2) is required to switch back to the original sampling rate. After the first stage, the y_{low} can be further decomposed using the same arrangement that is used in the first level. This higher decomposition will generate frequencies separated by an octave as shown in Fig. 4. Whichalso shows the dyadic filter bank of the multi-level DWT (Raouf *et al*., 2014). The DWT functions $G_0[]$ and $G_1[]$ suggest that the incoming signal will be transformed to orthogonal frequencies in the rate of $f/2^k$ where k = 1, 2, ..., K is the number of analysis levels. The reconstruction of the original signal x[n] from its DWT components can be accomplished by reversing the operations of Fig. 4. This is called Inverse DWT (IDWT). The reconstruction process is shown in Fig. 5. The reconstruction functions H_0 and H_1 are the inverse for the analyzing functions G_0 and G_1. The resultant signal $\hat{x}[n]$ is an estimate for the original signal x[n]. In reconstruction filter, the sampling rate is increased by a factor of 2(↑2) to reverse the decimation process.

Although, this operation might seem identical to FFT but the difference is that the frequency coming from the first HPF branch y^k_{high} maintains its frequency along the analysis. The DWT can be modified to be identical to FFT and further increases the final signal PSD concentration. The modification comes from decomposing y^1_{high} in the same manner y^1_{low} at every stage. This analysis is called Discrete Wavelet Packet Transform DWPT. The filters used for DWPT and Inverse DWPT (IDWPT) are shown in Fig. 6 and 7 respectively (Ezra *et al*., 2016; Chopra and Gupta, 2011; Mota *et al*., 2005; Percival and Walden, 2000).

From Fig. 6, it can be seen that the discrete signal x[n] is convolved with the analyzing filter resulting in transporting the incoming signal to new frequency values ($f/2_k$). Unlike the DWT filter, the DWPT has

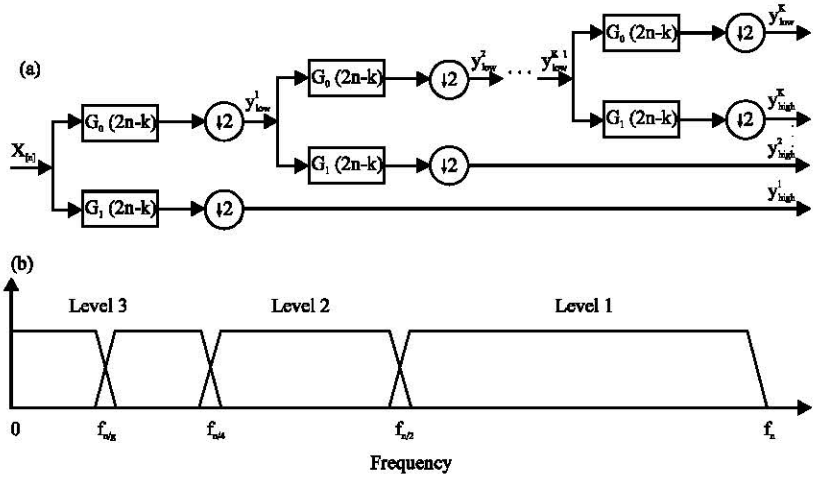

Fig. 4a: The dyadic filter banks and b) The LPF filter response

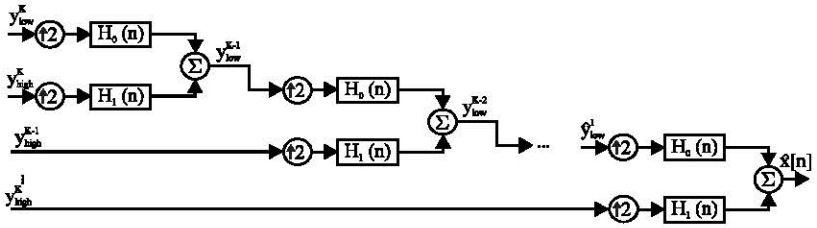

Fig. 5: The reconstruction filter (IDWT)

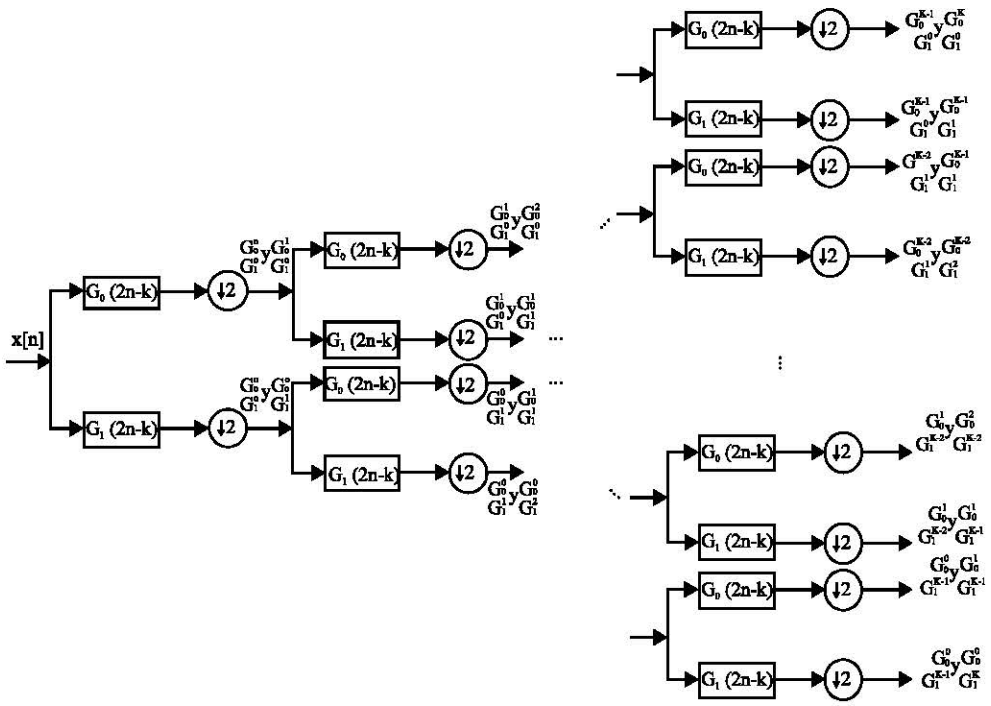

Fig. 6: DWPT analysis filter

equally sized filter banks and by this the DWPT resembles the FFT in its effect. Thus, the IFFT can be replaced with IDWPT and likewise the FFT with DWPT. To generate the orthonormal subcarriers using IDWPT, consider Eq. 6 and by using Mallat's Pyramid Algorithm (MPA) (Mallat, 1989) used for Multi-Resolution Analysis (MRA) then Eq. 6 can be written as:

$$y(t)=\sum_{k=-\infty}^{\infty}a_{j_0}(k)\Phi_{j_0}(t-k)+\sum_{j=j_0}^{\infty}\sum_{k=-\infty}^{\infty}b_j(k)\Psi_j(2^m t-k) \quad (7)$$

Where:

$$a_j(k)=\sum_m h(m-2k)a_{j+1}(m) \quad (8)$$

$$b_j(k)=\sum_m g(m-2k)b_{j+1}(m) \quad (9)$$

In Eq. 9 $g(\cdot)$ is called the wavelet coefficient function and is related to $h(\cdot)$ by Eq. 9 to maintain orthogonality:

$$g(k)=(-1)^k h(1-k) \quad (10)$$

Then for a scaling function of order N:

$$g(k)=(-1)^k h(N-1-k) \quad (11)$$

Hence, the dilation equation can be written as:

$$\Phi(t)=\sqrt{2}\sum_{k=0}^{N-1}h(k)\Phi(2t-k) \quad (12)$$

The wave let can be produced as:

$$\Psi(t)=\sum_{k=0}^{N-1}(-1)^k h(k)\Phi(2t+k-N+1) \quad (13)$$

Therefore, using MPA and extending it to the DWPT, series of x[n] vector can be analyzed using the following transformation matrix for L number of stages (Mehmood *et al*., 2017; Riju *et al*., 2015; Lipinski and Yatsymirskyy, 2008; Ul Hasan *et al*., 2013; Chrysafis and Ortega, 1999):

$$A=\begin{bmatrix}
h(0) & h(1) & h(2) & h(3) & \cdots & h(L-1) & 0 & 0 & \cdots & 0 & 0\\
0 & 0 & h(0) & h(1) & h(2) & h(3) & \cdots & h(L-1) & 0 & \cdots & 0\\
\vdots & \vdots & \vdots & \vdots & \vdots & \vdots & \vdots & \vdots & \vdots & \vdots & \vdots\\
h(4) & \cdots & h(L-1) & 0 & 0 & \cdots & 0 & h(0) & h(1) & h(2) & h(3)\\
h(2) & h(3) & \cdots & h(L-1) & 0 & 0 & \cdots & 0 & 0 & h(0) & h(1)\\
g(0) & g(1) & g(2) & g(3) & \cdots & g(L-1) & 0 & 0 & \cdots & 0 & 0\\
0 & 0 & g(0) & g(1) & g(2) & g(3) & \cdots & g(L-1) & 0 & \cdots & 0\\
\vdots & \vdots & \vdots & \vdots & \vdots & \vdots & \vdots & \vdots & \vdots & \vdots & \vdots\\
g(4) & \cdots & g(0) & 0 & \cdots & 0 & 0 & g(0) & g(1) & g(2) & g(3)\\
g(2) & g(3) & \cdots & g(L-1) & 0 & 0 & \cdots & 0 & 0 & g(0) & g(1)
\end{bmatrix} \quad (14)$$

By substituting Eq. 11 in 13, the transformation matrix becomes:

$$A=\begin{bmatrix}
h(0) & h(1) & h(2) & h(3) & \cdots & h(L-1) & 0 & 0 & \cdots & 0 & 0\\
0 & 0 & h(0) & h(1) & h(2) & h(3) & \cdots & h(L-1) & 0 & \cdots & 0\\
\vdots & \vdots & \vdots & \vdots & \vdots & \vdots & \vdots & \vdots & \vdots & \vdots & \vdots\\
h(4) & \cdots & h(L-1) & 0 & 0 & \cdots & 0 & h(0) & h(1) & h(2) & h(3)\\
h(2) & h(3) & \cdots & h(L-1) & 0 & 0 & \cdots & 0 & 0 & h(0) & h(1)\\
h(L-1) & -h(L-2) & h(L-3) & \cdots & h(1) & -h(0) & 0 & 0 & \cdots & 0 & 0\\
0 & 0 & h(L-1) & -h(L-2) & h(L-3) & \cdots & h(1) & -h(0) & 0 & \cdots & 0\\
\vdots & \vdots & \vdots & \vdots & \vdots & \vdots & \vdots & \vdots & \vdots & \vdots & \vdots\\
h(L-5) & \cdots & h(0) & 0 & \cdots & 0 & 0 & h(L-1) & -h(L-2) & h(L-3) & -h(L-4)\\
h(L-3) & \cdots & h(1) & -h(0) & 0 & 0 & \cdots & 0 & 0 & h(L-1) & -h(L-2)
\end{bmatrix} \quad (15)$$

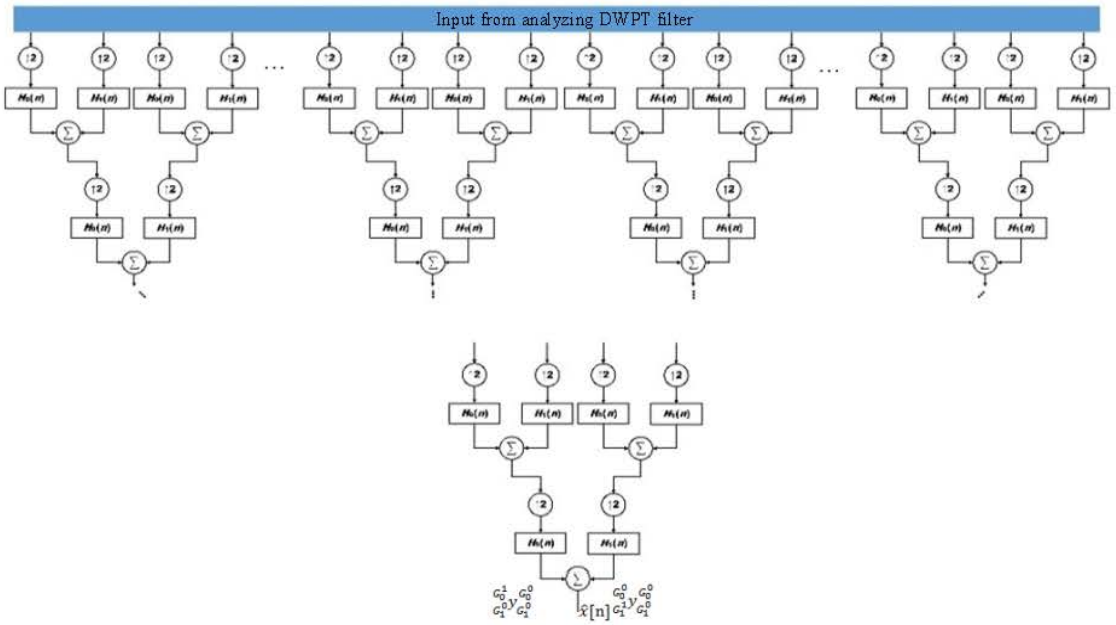

Fig. 7: IDWPT composition filter

$$C = \begin{bmatrix} h(0) & 0 & 0 & \cdots & 0 & 0 & h(2) & h(L-1) & 0 & 0 & 0 & h(1) \\ h(1) & 0 & 0 & \cdots & 0 & 0 & \vdots & \vdots & 0 & 0 & 0 & -h(0) \\ \vdots & h(0) & 0 & \cdots & 0 & 0 & h(L-1) & h(1) & h(L-1) & 0 & 0 & 0 \\ h(L-1) & h(1) & 0 & \cdots & 0 & 0 & 0 & -h(0) & \vdots & 0 & 0 & 0 \\ 0 & \vdots & h(0) & \cdots & \vdots & 0 & 0 & 0 & h(1) & h(1) & \vdots & 0 \\ 0 & h(L-1) & h(1) & \cdots & 0 & 0 & 0 & 0 & -h(0) & \vdots & 0 & 0 \\ 0 & 0 & \vdots & \cdots & 0 & \vdots & 0 & 0 & 0 & -h(1) & 0 & \vdots \\ 0 & 0 & h(L-1) & \cdots & 0 & 0 & 0 & 0 & 0 & h(0) & 0 & 0 \\ 0 & 0 & 0 & \cdots & 0 & 0 & 0 & 0 & 0 & 0 & 0 & 0 \\ \vdots & 0 & 0 & \cdots & 0 & 0 & 0 & \vdots & 0 & 0 & 0 & 0 \\ 0 & \vdots & 0 & \cdots & h(0) & 0 & \vdots & 0 & \vdots & 0 & h(L-1) & 0 \\ 0 & 0 & \vdots & \cdots & h(1) & 0 & 0 & 0 & 0 & \vdots & \vdots & h(L-1) \\ 0 & 0 & 0 & \cdots & \vdots & h(0) & 0 & 0 & 0 & 0 & -h(1) & \vdots \\ 0 & 0 & 0 & \cdots & h(L-1) & h(1) & 0 & 0 & 0 & 0 & h(0) & h(2) \end{bmatrix}$$

Using the orthonormal property, the reconstruction matrix is simply the transpose of the analysis function. Hence, at the construction side the following matrix is used: the following steps summarizes the analysis of 1-dimension Vector V of length D:

- Construct an input vector X from V such that its length is of power of 2 (2^n)
- Construct the analyzing matrix A and multiply X with A
- If the leftover of V is not equal to 2^m, then pad the remaining vector with zeros and carry on the multiplication

The reconstruction is done as follows:

- Collect the incoming vector Y of power 2^m
- Construct the C and multiply Y with C
- After completing the process, remove any padded zeros

The matrix C will ensure neutralizing the effect of DWPT matrix A due to their mutual orthogonality. In OFDM, the IFFT section can be replaced by the IDWPT (matrix C), so that, the incoming frames will be transformed to orthogonal subcarriers with equal spacing while at the receiver side, the matrix A will be used to recover the transformed frames by the transmitter (Fig. 7).

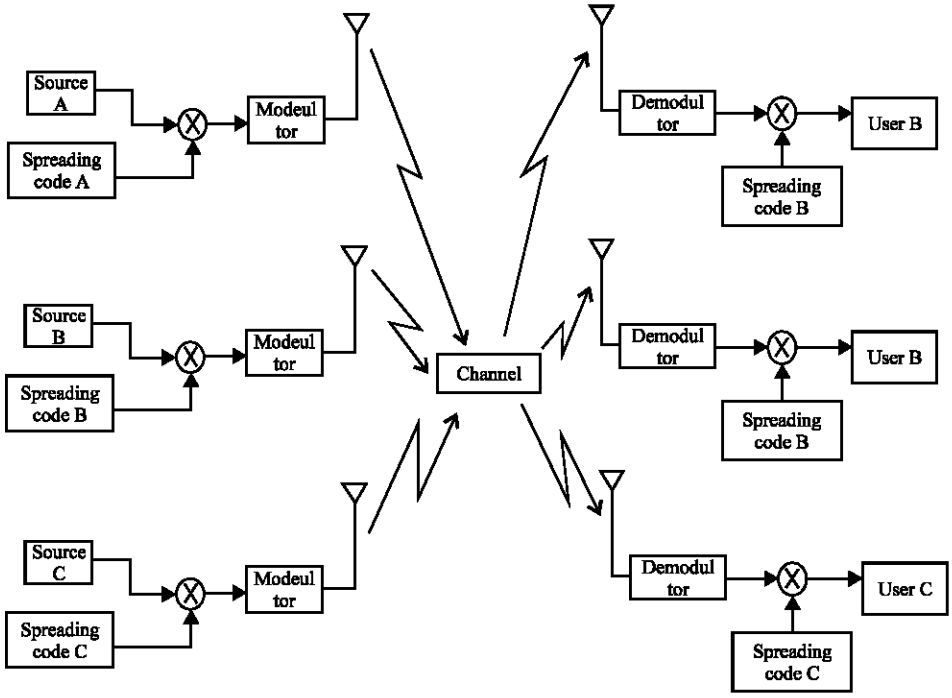

Fig. 8: A typical CDMA system block diagram

OFDM and Code Division Multiple Access (CDMA): The OFDM can ensure complete separation for overlapped channels due to the orthogonality property. This property is tightly adhered to the location of subcarriers. If the locations of these subcarriers are dispositioned, then the orthogonality will fall apart and the system will experience the Inter Channel Interference ICI (Gayvoronskiy and Danilchuk, 2017; Shi *et al*., 2017a, b). The ICI will reduce the system performance due to the decrease in the signal quality. The dispositioning can occur due to many reasons such as equipment aging, heat, nonlinearity in the amplifiers, dispersive channels multi path and lack of synchronicity between the transmitter and receiver. Therefore, certain measures should be taken in order to counter act the effect of no ideal subcarrier generation. One of these measures is the CDMA (Verma *et al*., 2016). The CDMA is built upon the Spread Spectrum System SSS technology by which it allows all the users to use the channel all the time. This comes from the fact that the CDMA uses orthogonal spreading code to distinguish between users. This strong feature will strongly serve the purpose of reducing the ICI in OFDM system. A typical CDMA is shown in Fig. 8 (Simon, 2002).

In the CDMA, each user is assigned a PN-sequence (Pseudo noise). These sequences are generated using Linear Feedback Shift Registers (LFSR). The word Pseudo comes from the fact that the sequence will repeat itself after a period of time depending on the LFSR constraint length. The generated PN pulses are almost random, hence, they inherit the noise samples properties that are independent of each other. Thus, the Auto Correlation function ACF of the PN sequence has the property given in Eq. 17 (Lee and Miller, 1998).

$$ACF(t)=\int PN(t)PN(t+\tau)\,d\tau=\begin{cases}1 & \tau=0\\ -\frac{1}{N} & \tau\neq 0\end{cases} \quad (17)$$

Where:
N = The maximal length and equals to 2^n-1
n = The LFSR constraint length

The ACF is almost like the ACF of the noise as N→∞ the ACF→0. This implies that when the PN sequence is aligned with itself then ACF will have 1 value otherwise sequence will annihilate the incoming data. Unfortunately, the PN-sequence has poor Cross Correlation Function (CCF) that's why different arrangements were invented to overcome this problem.

One of the widely used code generator is the Gold code generator. This generator is composed of two banks of preferred primitive sequences realized by two LFSRs as shown in Fig. 9. The output of these LFSRs is XORed to generate the final sequence.

If the sequences are chosen carefully, then the CCF will have only three states which are {-t (n)/N, -1/N, t (n)-2/N}, where:

$$t(n)=\begin{cases}1+2^{\frac{n+1}{2}} & \text{for n odd}\\ 1+2^{\frac{n+2}{2}} & \text{for n even}\end{cases} \quad (18)$$

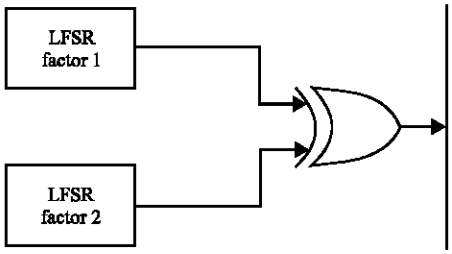

Fig. 9: Gold code sequence generator

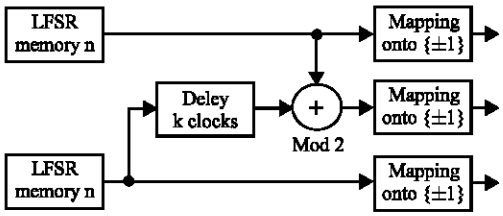

Fig. 10: Gold code generator with delay bank

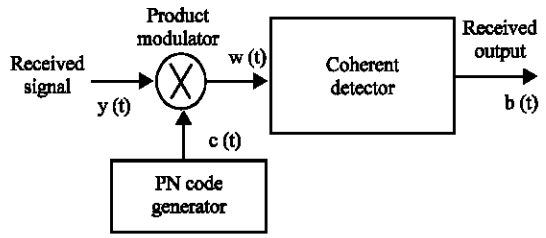

Fig. 11: A detailed spread spectrum demodulator

To increase the possible codes that can be generated using the arrangement in Fig. 9, a delay bank can be used with length 0→N-1 as shown in Fig. 10 (Simon, 2002). The delay bank, the middle line, can ensure that the possible number of generated codes (Gold code group) reaches maximum of 2^n depending on the length of delay bank. All these codes will have a CCF value as given by Eq. 18. This technique for generating spreading codes is used by this study to spread the mapped substreams of the OFDM. At the receiver side, the incoming streams are multiplied by the same Gold code group and then passed through a coherent detector as shown in Fig. 11 which is an elaboration for Fig. 8 receiver side. Let the transmitted OFDM signal to be s (t), then received signal y (t) is:

$$y(t)=s(t)\check{c}(t)+N(t) \tag{19}$$

Where:

$\check{c}$ (t) = The spreading code at the transmitter side

N (t) = The impairments from the channel like noise or jamming or interference or multipath

$$N(t)=n(t)+J(t)+\sum_{i=1}^{M}s(t-\tau_i)\check{c}(t-\tau_i) \tag{20}$$

Where:

n(t) = The AWGN noise

j(t) = The jamming signal

τ = The time delay due to multipath

M = The number of possible multipath signals

After multiplying y(t) by c(t) then output signal b(t) of the coherent detector for the input w(t) is:

$$b(t)=\frac{1}{T_b}\left[\int_0^{T_b}s(t)\check{c}(t)c(t)\,dt+\int_0^{T_b}N(t)c(t)\,dt\right] \tag{21}$$

Due to the orthogonality property then the first integration will not be zero if and only if $\check{c}(t) \equiv c(t)$. The second part of the integration which contains the impairments will be as follows:

$$P(t)=\frac{1}{T_b}\int_0^{T_b}c(t)\left[n(t)+J(t)+\sum_{i=1}^{M}s(t-\tau_i)\check{c}(t-\tau_i)\right]dt=$$
$$\frac{1}{T_b}\left[\int_0^{T_b}c(t)n(t)dt+\int_0^{T_b}c(t)J(t)dt+\int_0^{T_b}c(t)\left(\sum_{i=1}^{M}s(t-\tau_i)\check{c}(t-\tau_i)\right)dt\right]=$$
$$\frac{1}{T_b}\left[\int_0^{T_b}c(t)n(t)dt+\int_0^{T_b}c(t)J(t)dt+\sum_{i=1}^{M}\left(\int_0^{T_b}c(t)s(t-\tau_i)\check{c}(t-\tau_i)dt\right)\right] \tag{22}$$

The third integration in Eq. 22 will be zero assuming perfect independence between c(t) and any shifted version of it. Hence, the multipath will be nulled or practically, substantially reduced due to spreading process. The only left parts of the integration are the effect of AWGN noise and the jamming signal (burst noise). The spread code will not have a noticeable effect on the noise part and the noise PSD will be $N^0/2$. The remaining part is the jamming part. If the jamming signal has narrow bandwidth then c(t) will spread this power over a large bandwidth while accumulating the original signal. Thus, after the detector, the jamming is (Abu-Rgheff, 2007):

$$\overline{PSD_J}=\frac{PSD_J}{N} \tag{23}$$

Equation 22 states that the spread spectrum has higher immunity to jamming signal or burst noise than the casual system. This immunity depends on the maximal length of the spreading sequence and it's CCF. The SINR (Signal to Interference and Noise Ratio) for the CDMA system can be found to be:

$$SINR=\frac{1}{\frac{N_0}{2E_b}+\frac{(K-1)T_c}{3T_b}} \tag{24}$$

Where:
N_0 = The AWGN PSD
E_b = The Energy per bit
K = The number of users
T_c, T_b = The chip and bit durations, respectively

Therefore, the Probability of error P_e is:

$$P_e = Q\left(\sqrt{SINR}\right) = Q\left(\sqrt{\frac{1}{\frac{N_0}{2E_b} + \frac{(K-1)}{3N}}}\right) \quad (25)$$

When $K \neq 1$, $E_b = 8$ and $N>1$, Eq. 25 will become the equation for the irreducible error. This means that there is a certain limit, no matter how much power is used in the transmission ($E_b = 8$), the error will remain constant.

Despite the irreducible error, adding the CDMA to the OFDM will enhance its performance immensely according to Eq. 23.

The dispersive channel effect: The practical channels are usually imperfect and thus are described using its impulse response. Assume a Frequency Selective Fading Channel FSFCh of length L then the received signal r(t) is given in Eq. 26, assuming noise free channel (Proakis and Salehi, 2008; Pischella and Ruyet, 2015):

$$r(n) = \sum_{k=0}^{L-1} h(k)s(n-k) \quad (26)$$

where, s(n) = The transmitted signal. Equation 26 shows that the channel with such Channel Impulse Response (CIR) will cause Inter-Symbols Interference (ISI) or in the case of OFDM will be worse which is Inter-Block Interference (IBI) or Inter-Channel Interference (ICI). If 2 blocks of data $U = [u_1, u_2, \ldots, u_N]$ and $V = [v_0, v_1, \ldots, v_{N-1}]$ are to be transmitted consecutively through an FSFC then after the first block U is completed the contents of the channel is:

$$r(n) = \sum_{k=0}^{L-1} h(k)U(n-k) \quad (27)$$

When the first symbol of V starts to enter the channel, then the received signal will be:

$$r(n) = V(0)h(0) + \sum_{k=1}^{L-1} h(k)U(n-k) \quad (28)$$

Equation 28 shows what is meant by IBI. This serious problem can be cured using the Cyclic Prefix (CP). The CP is simply adding L symbols copied from the end of a block to its beginning. The final length for the prefixed block is N+L. The U block after prefixing will be $U = [u_{N-L}, u_{N-L-1}, \ldots, u_{N-1}, u_0, u_1, \ldots, u_{N-1}]$. When such block is transmitted through the channel of Eq. 27, then the linear convolution is converted to cyclic convolution (Hanzo *et al*., 2004):

$$r(t) = s(t) \bar{\times} h(t) \overset{\text{Cyclic Prefix}}{\Rightarrow} r(t) = s(t) \otimes h(t) \quad (29)$$

Where:
$\bar{\times}$ = Linear convolution
$\otimes$ = Cyclic convolution

Equation 27 will pass through an FFT (DPWT) circuit then the right hand side of Eq. 29 will be:

$$R(n) = S(n)H(n) \quad (30)$$

Bearing in mind that the input to the FFT circuit is $s[n] = [S(N-L)\ S(N-L-1), \ldots, S(N-1)\ S(0), \ldots, S(N-1)\ h(n) = [h(0)\ h(1), \ldots, h(L-1)\ 0_L, \ldots, 0_{N+L-1})$ and the output will be R (n) = [R(0) R(1), ... , R(N+L-1). The FFT will pad zeros to h(k) in order to equate its length with s(n). The FFT of s(n) will reverse the IFFT of the symbols in the transmitter. Hence, for any symbol at k instant then R(k) = S (k) H (k) which means that the original symbols will only be affected by the channel response coefficients rather than the summation of the previously transmitted symbols. Therefore, Eq. 28 shows that the case is now not IBI or ICI due to FSFC anymore but rather a Frequency Flat Fading Channel FFFC which is simpler to be cured. This is the reason why the OFDM has supreme performance over the traditional communication systems. The advantages of CP are: first, it increases the system robustness because it provides copies of the symbols in case certain symbol was lost and the second is reducing the interference. The disadvantage comes from the reduction in channel capacity due to the repetition in the transmitted symbols.

Frequency flat fading channel and Space Time Block Code STBC: After converting the FSFC to FFFC as given above, it is convenient now to reduce the effect of the FFFC as much as possible to increase the signal quality. One of the methods used to overcome the FFFC effect is the M IMO-STBC (Bessate and Bouanani, 2016, Mehrizi and Mahboobi, 2017).

MIMO which stands for Multi-Input Multi-Output is a technique by which the symbol is transmitted through different paths (channels) in order to null the CIR. To ensure that the MIMO works the best, the CIR should be known and well tracked over time. Unfortunately, this situation may become complicated or sometimes unaffordable if the channel is not ergodic. For this reason,

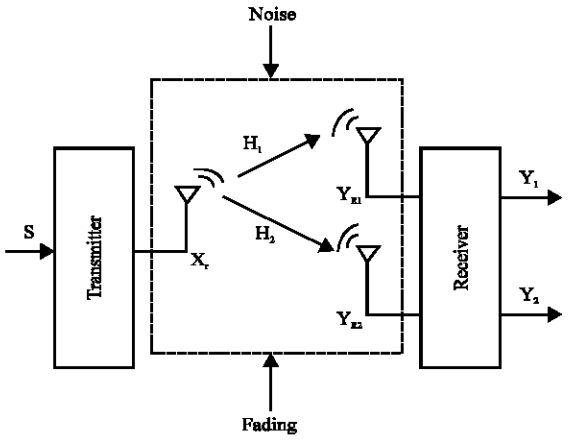

Fig. 12: A 2×1 SIMO system

this study adopted the Alamouti's STBC to avoid the continuous need to update the CIR (Kumar and Ravindra, 2016, Bahai *et al*., 2004).

The simplest form of Alamouti scheme is the MISO (Multiple-Input Single-Output) of 1×2 which means that the number of receiving antennas is 1 and the number of transmitting antennas is 2 as shown in Fig. 12.

Let two symbols x_1 and x_2 to be transmitted by this MISO over a two channels of CIR or sometimes called Channel State Information CSI of h_1 and h_2 then the received symbols at the first instant are:

$$y_1(t) [h_1\ h_2]\begin{bmatrix} x_1 \\ x_2 \end{bmatrix} + n_1(t) \tag{31}$$

At the second instance, the first antenna will transmit $x^*_2(t)$ and the second antenna will transmit $-x^*_2(t)$, *means conjugate, the received symbols at the second instance are:

$$y_2(t) = [h_1\ -h_2]\begin{bmatrix} x^*_2 \\ -x^*_1 \end{bmatrix} + n_2(t) \tag{32}$$

Taking the conjugate of Eq. 31 and arranging the result to look like:

$$y^*_2(t) = [h^*_2\ -h^1_*] + n_2(t) \tag{33}$$

where, $n_1(t)$ and $n_2(t)$: is the AWGN in the first and second transmission instances, respectively. Combining Eq. 30 with 32, it can be shown that:

$$\begin{bmatrix} y_1(t) \\ y^*_2(t) \end{bmatrix} = \begin{bmatrix} h_1 & h_2 \\ -h^*_2 & h^*_1 \end{bmatrix} \begin{bmatrix} n_1(t) \\ n^*_2(t) \end{bmatrix} \tag{34}$$

$$\text{Let } Y = \begin{bmatrix} y_1(t) \\ y^*_2(t) \end{bmatrix}, C_1 = \begin{bmatrix} h_1 \\ -h^*_2 \end{bmatrix}, C_2 = \begin{bmatrix} h_2 \\ -h^*_1 \end{bmatrix} \text{ and } N = \begin{bmatrix} n_1(t) \\ n^*_2(t) \end{bmatrix} \text{then } Y = [C_1 \quad C2] \begin{bmatrix} x_1(t) \\ x_2(t) \end{bmatrix} + \tag{35}$$

Interestingly $\{C^H_1, C_2) = 0$ which means they are orthogonal. That is why the Alamouti code is called Orthogonal STBC (OSTBC). Thus, by multiplying Y by $\frac{C^H_1}{\|C_1\|}N$ then:

$$\frac{C^H_1}{\|C_1\|} Y = \frac{C^H_1}{\|C_1\|}[C_1 \quad C_2]\begin{bmatrix} x_1(t) \\ x_2(t) \end{bmatrix} + N\} = \|C_1\| x_1(t) + 0 + \frac{C^H_1}{\|C_1\|} N \tag{37}$$

Similarly, if Y is multiplied by $\frac{C^H_2}{\|C_2\|}N$:

$$\frac{C^H_2}{\|C_1\|} Y = 0\, \|C_2\| x_2(t) + \frac{C^H_2}{\|C_1\|} N \tag{38}$$

This means that the ISI can be nulled. Assume the power contained in $x_1(t)$ is equal to the power contained in $x_2(t)$, then the SNR for the Alamouti OSTBC can be shown to be (Jafarkhani, 2005, Giannakis, 2007):

$$SNR = \frac{1}{2}\|h_i\| \frac{P}{\sigma^2} \tag{39}$$

Where:
σ^2 = The AWGN variance (power)
i = The ith symbol

Equation 36 shows that the Alamouti ensures no ISI but at the same time the SNR is half the SNR of the Maximal Ratio Combiner (MRC). The elegance of Alamouti code is that, unlike the MRC, it requires no pre-defined CSI in order to ensure the absence of ISI as it works anonymously. Using the above approach, the Alamouti OSTBC can be extended from MISO to MIMO easily (Mecklenbrauker and Rupp, 2004; Rindani and Rindani, 2015). Assume:

$$H_1 \begin{bmatrix} h_1 & h_2 \\ -h^*_2 & h_1 \end{bmatrix} \tag{40}$$

$$H_1 \begin{bmatrix} h_3 & h_4 \\ -h^*_4 & h_3 \end{bmatrix} \tag{41}$$

Then the Alamouti for a 4×4 can be simply constructed by repeating Eq. 38 orthogonally or in other words like the Walsh-Hadamard code matrix. Thus, for a 4×4 system:

$$H_3\begin{bmatrix} H_1 & H_2 \\ -H_2^* & H_1 \end{bmatrix} \quad (42)$$

Then constructing an H_4 as in Eq. 38 and applying it to Eq. 39 to include H_3 and H_4, a 4×4 system is generated and henceforth for higher MIMO levels. Thus, using this procedure for the 4×4, the symbol generation and timings are shown in Table 1 and 2.

Table 1: Transmitted Symbols Timings for MIMO 4×4

Time slot	T_x^1	T_x^2	T_x^3	T_x^4
T_0	s_1	s_2	s_3	s_4
T_1	$-s_2$	s_1	$-s_4$	s_3
T_2	$-s_3$	s_4	s_1	$-s_2$
T_3	$-s_4$	$-s_3$	s_2	s_1
T_4	s_1^*	s_2^*	s_3^*	s_4^*
T_5	s_2^*	s_1^*	s_4^*	s_3^*
T_6	s_3^*	s_4^*	s_1^*	s_2^*
T_7	s_4^*	s_3^*	s_2^*	s_1^*

Table 2: OFDM physical layer simulation settings

	Mobile MC-DS-CDMA scalable				
Parameters	----------OFDMA-PHY----------				
FFT or DWT size	128	512	1024	2048	
Number of used data subcarriers	64	180	360	720	
Modulation types	QPSK				
Cyclic prefix	1/16				
Channel bandwidth (MHz)	20	20	20	20	20

RESULTS AND DISCUSSION

The suggested system combines all the above concepts and integrates them into a single communication system in order to provide enough protection for the signals during their trip from source to destination. The system is shown in Fig. 13. In the beginning, the signals

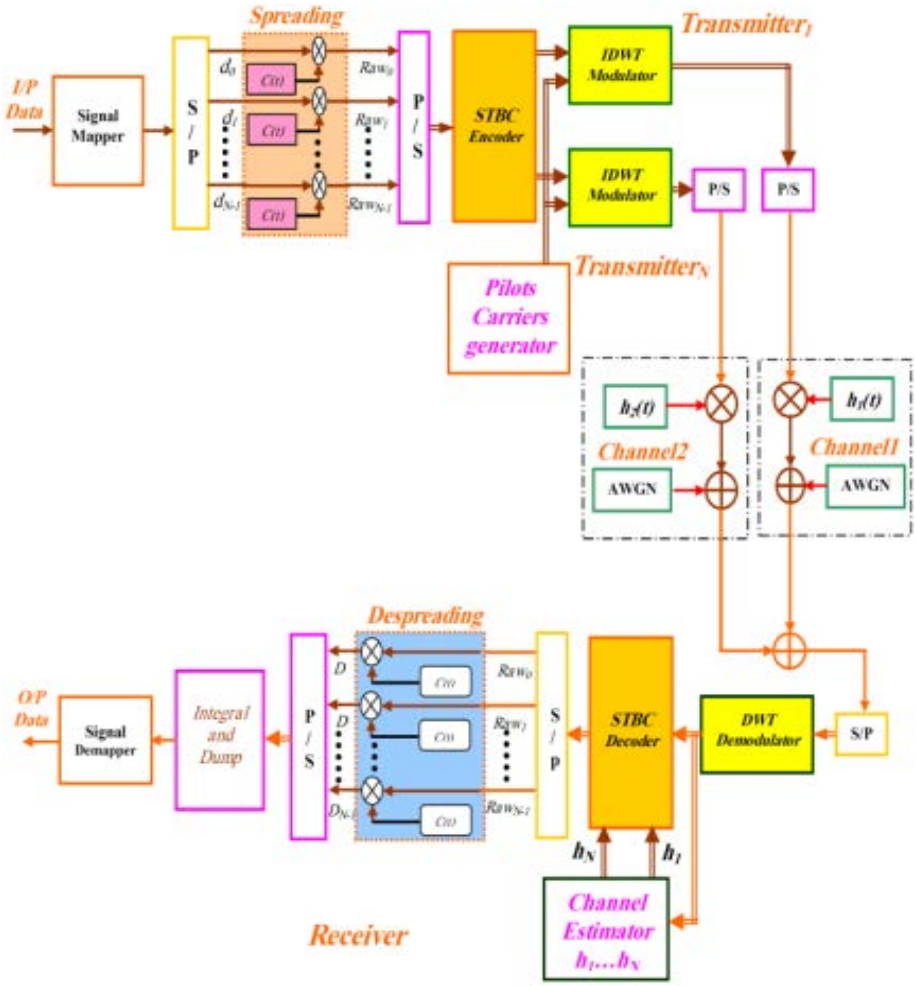

Fig. 13: The complete suggested communication system

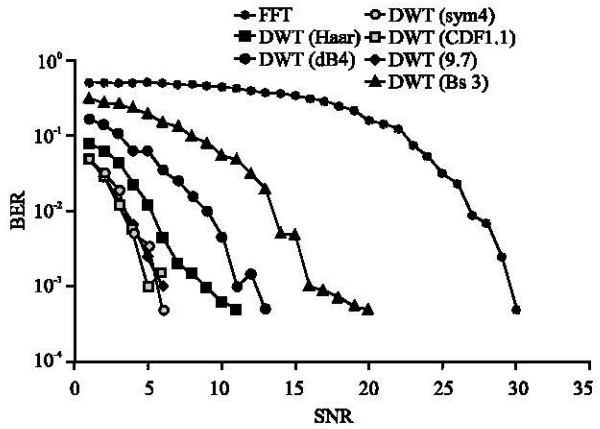

Fig. 14: BER performance of STBC DWT-mobile MC-DS-CDMA in AWGN channel model-128 subcarriers

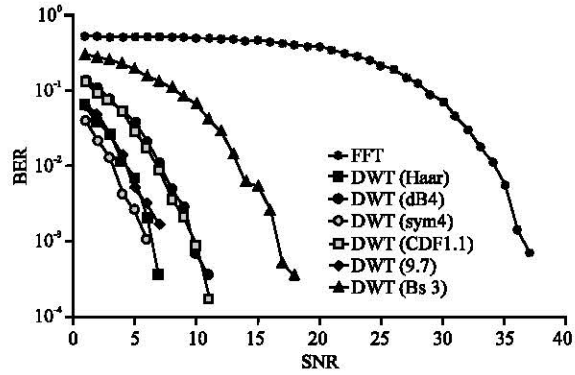

Fig. 15: BER performance of STBC DWT-mobile MC-DS-CDMA in AWGN channel model-512 subcarriers

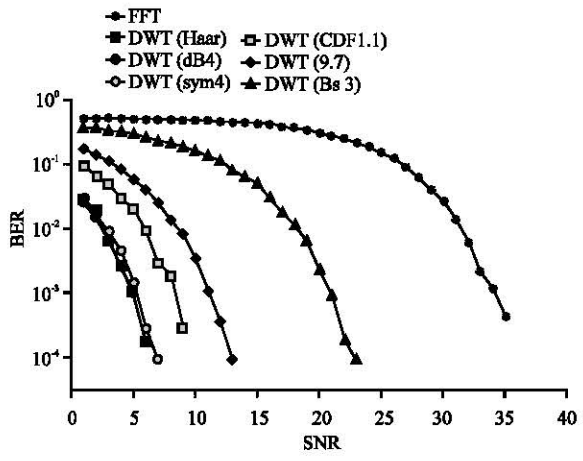

Fig. 16: BER performance of STBC DWT-mobile MC-DS-CDMA in AWGN channel model-1024 subcarriers

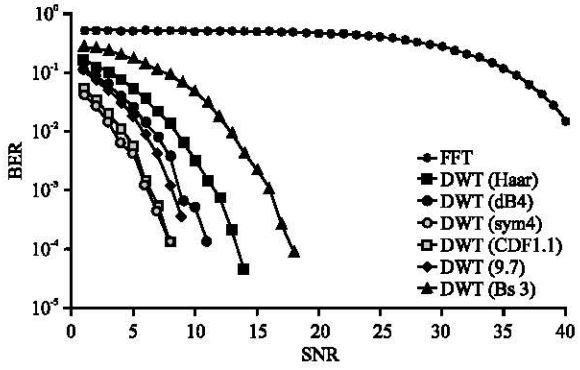

Fig. 17: BER performance of STBC DWT-mobile MC-DS-CDMA in AWGN channel model-128 subcarriers

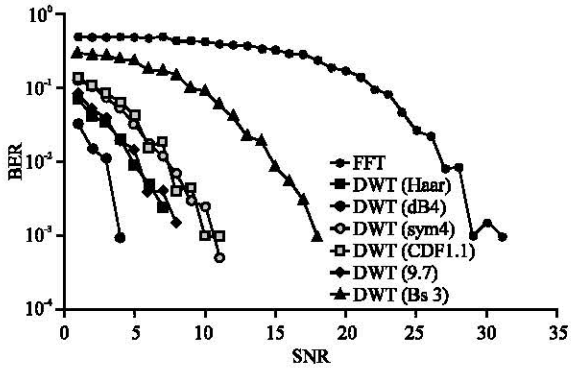

Fig. 18: BER performance of STBC DWT-mobile MC-DS-CDMA in AWGN channel model-512 subcarriers

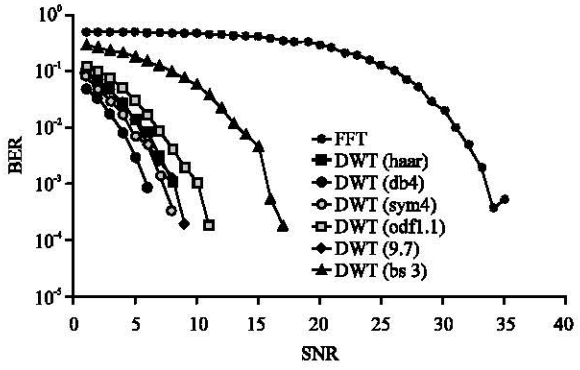

Fig. 19: BER performance of STBC DWT-Mobile MC-DS-CDMA in AWGN channel model-512 subcarriers

are mapped using QPSK scheme then the stream is divided to sub-streams using the Serial to Parallel circuit (S/P) (Fig. 14-25). An OSTBC is added then the resultant stream is fed to IDWPT section to generate the

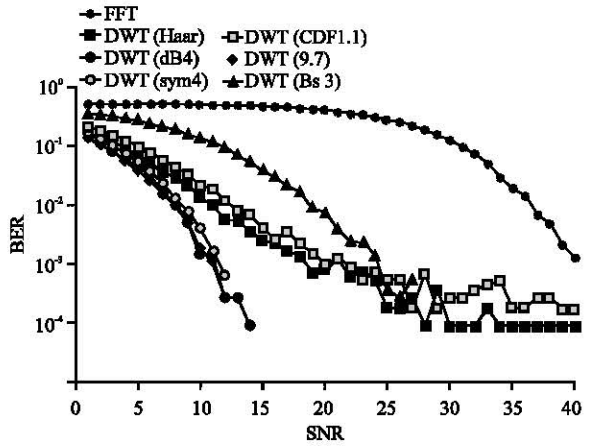

Fig. 20: BER performance of STBC DWT-mobile MC-DS-CDMA in AWGN channel model-1024 subcarriers

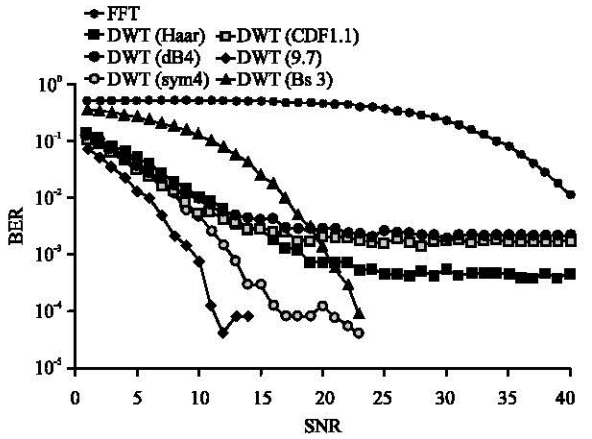

Fig. 21: BER performance of STBC DWT-mobile MC-DS-CDMA in AWGN channel model-2048 subcarriers

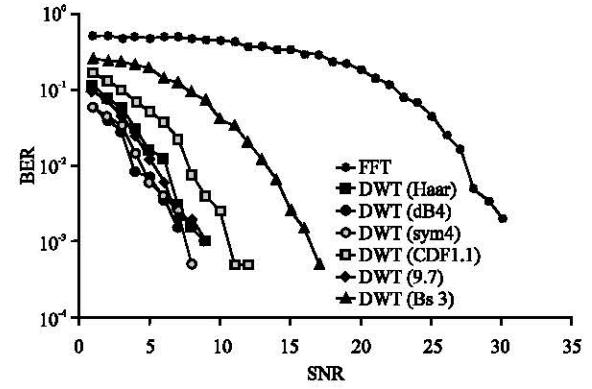

Fig. 22: BER performance of STBC DWT-mobile MC-DS-CDMA in AWGN channel model-128 subcarriers

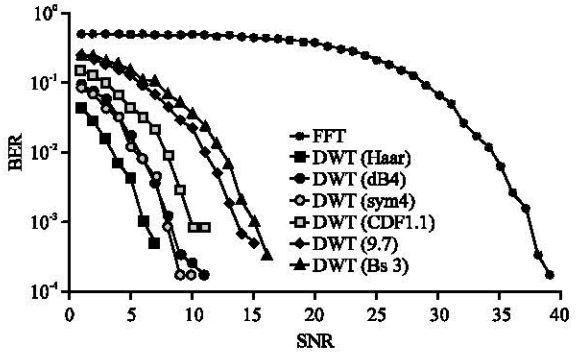

Fig. 23: BER performance of STBC DWT-mobile MC-DS-CDMA in AWGN channel model-512 subcarriers

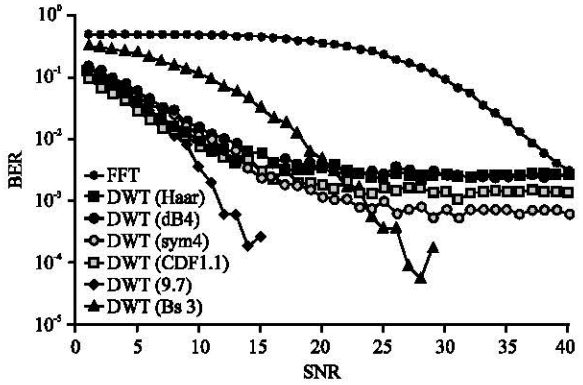

Fig. 24: BER performance of STBC DWT-mobile MC-DS-CDMA in AWGN channel model-1024 subcarriers

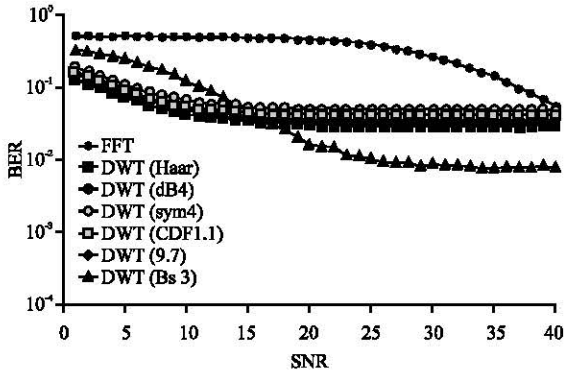

Fig. 25: BER performance of STBC DWT-mobile MC-DS-CDMA in AWGN channel model-2048 subcarriers

orthogonal subcarriers. A copied version of these subcarriers is merged with the final signal before the conversion to serial using parallel to serial circuit. These pilots are used for synchronization and estimating the CSI

of the channel in order to provide the necessary equalization if needed. This serial stream is then fed to a MIMO of 4×4 according to Table 1 and then sends over the channel. The transmitter is assumed to be a mobile travelling at speeds 2, 45 and 100 km/h creating Maximum Doppler Shift (MDS) of 10.7, 241.7 and 537 Hz, respectively. The channel is FFFD Rayleigh channel with AWGN. The number of transmitted bits per test is (102400 bit) coming from (100 packet*64 characters*16 bit/char). The used mother wavelets are: Haar, Daubechies = dB4, Symlets = sym4, Cohen Daubechies-Feauveau = CDF and B-spline 3 = Bs3. The results are as follows: MDS 10.7 Hz, the BER are shown in Fig. 14-24.

CONCLUSION

The above results showed that the IDWPT/DWPT has a better performance than the IFFT/FFT over all channels and settings. This justifies the assumption that the DWPT has higher concentrated signal PSD. But in all cases, the BER increases with increase of bit rate and this event is inevitable. The Doppler shift has high impact on system performance as it increases due to the motion of the mobile station. The higher the Doppler shift the worse the performance. The Doppler shift disturbs the positions of the orthogonal subcarriers which derives the orthogonality that is related to the frequency difference between the adjacent carriers, to lose its effect. Hence, the pilots were transmitted to resynchronize the system but even at certain bit rate and motion speed they lose their effectiveness. The irreducible error appears after the speed is high enough to cause an irrecoverable errors. Neither the STBC nor the CDMA are now able to track and reverse the Doppler shift effect. The Bs3 has the worst BER performance among the tested mother wavelet functions while the others are competing on the first place. This indicates that not every mother wavelet is adequate to replace the IFFT in the transmitter. Nevertheless, it can be noticed that the wavelets haveno close relation to the bit ratewhich is clearly seen from the exchange of ratings. Nevertheless, there are wavelets that score the worst of performance like Bs3. Therefore, the selection for the wavelet should be carefully done and not at random.

REFERENCES

Abu-Rgheff, M.A., 2007. Introduction to CDMA Wireless Communications. 1st Edn., Elsevier, Amsterdam, Netherlands, ISBN:978-0-75-065252-0, Pages: 511.

Bahai, A. and B. Saltzberg, 2002. Multi-Carrier Digital Communications Theory and Applications of OFDM. Kluwer Academic/Plenum Publishers, New York, USA.,.

Bahai, A.R.S., B.R. Saltzberg and M. Ergen, 2004. Multi-Carrier Digital Communications Theory and Applications of OFDM. 2nd Edn., Springer, Berlin, Germany, ISBN:9780387225753, Pages: 411.

Bessate, A. and F.E. Bouanani, 2016. A new performance results of MIMO system with orthogonal STBC over independent and identical weibull fading channels. Proceedings of the International Conference on Advanced Communication Systems and Information Security (ACOSIS'16), October 17-19, 2016, IEEE, Marrakesh, Morocco, ISBN:978-1-5090-6228-7, pp: 1-7.

Bodhe, R., S. Joshi and S. Narkhede, 2012b. Performance comparison of FFT and DWT based OFDM and selection of mother wavelet for OFDM. Intl. J. Comput. Sci. Inf. Technol., 3: 3993-3997.

Bodhe, R., S. Narkhede and S. Joshi, 2012a. Design of simulink model for OFDM and Comparison of FFT-OFDM and DWT-OFDM. Intl. J. Eng. Sci. Technol., 4: 1914-1924.

Chen, X., S. Peng, J.Z. Huang, F. Nie and Y. Ming, 2017. Local purtree spectral clustering for massive customer transaction data. IEEE.Intell.Syst., 32: 37-44.

Chrysafis, C. and A. Ortega, 1999. An algorithm for low memory wavelet image compression. Proceedings of the International Conference on Image Processing (ICIP'99) Vol. 3, October 24-28, 1999, IEEE, Kobe, Japan, pp: 354-358.

Debnath, L. and F.A. Shah, 2015. Wavelet Transforms and their Applications. 2nd Edn., Birkhauser Verlag, Basel, Switzerland, ISBN:978-0-8176-8417-4, Pages: 545.

Ejaz, W., M.K. Atiq and H.S. Kim, 2013. Recursive pyramid algorithm-based discrete wavelet transform for reactive power measurement in smart meters. Energies, 6: 4721-4738.

Ezra, Y.B., A. Zadok, R. Califa, D. Munk and B.I. Lembrikov, 2016. All-optical wavelet-based orthogonal frequency division multiplexing system based on silicon photonic integrated components. IET. Optoelectron., 10: 44-50.

Faisal, C.N., M. Gonzalez-Rodriguez, D. Fernandez-Lanvin and J.D. Andres-Suarez, 2017. Web design attributes in building user trust, satisfaction and loyalty for a high uncertainty avoidance culture. IEEE. Trans. Hum. Mach. Syst., 47: 847-859.

Gayvoronskiy, D.V. and E.A. Danilchuk, 2017. Analysis of multiple-access interference for CDMA signals. Proceedings of the IEEE Russian Conference on Young Researchers in Electrical and Electronic Engineering (EIConRus'17), February 1-3, 2017, IEEE, St. Petersburg, Russia, ISBN:978-1-5090-4866-3, pp: 144-145.

Giannakis, G.B., 2007. Space-Time Coding for Broadband Wireless Communications. John Wiley & Sons, New York, USA., ISBN-13:978-0-471-21479-3, Pages: 354.

Jafarkhani, H., 2005. Space-time Coding: Theory and Practice. 1st Edn., Cambridge University Press, UK., ISBN-10: 0521842913.

John, G.P., 2008. Digital Communications. 5th Edn., McGraw-Hill, New York, USA., ISBN:9780071263788, Pages: 1150.

Kaur, D. and D. Garg, 2015. Variable bid fee: An online auction shill bidding prevention methodology. Proceedings of the IEEE International Conference on Advance Computing (IACC'15), June 12-13, 2015, IEEE, Banglore, India, ISBN:978-1-4799-8048-2, pp: 381-386.

Kaur, P., M. Goyal and J. Lu, 2017. A comparison of bidding strategies for online auctions using fuzzy reasoning and negotiation decision functions. IEEE. Trans. Fuzzy Syst., 25: 425-438.

Khan, A., M.R. Usman, M.B. Shahab and S.Y. Shin, 2016. Performance comparison of DFT and DWPT based OFDM system using 64 DAPSK. Proceedings of the International Conference on Smart Green Technology in Electrical and Information Systems (ICSGTEIS'16), Octocber 6-8, 2016, IEEE, Bali, Indonesia, ISBN:978-1-5090-2691-3, pp: 59-63.

Khan, S.I. and A.S.M.L. Hoque, 2017. Health data integration with Secured Record Linkage: A practical solution for Bangladesh and other developing countries. Proceedings of the International Conference on Networking, Systems and Security (NSysS'17), January 5-8, 2017, IEEE, Dhaka, Bangladesh, ISBN:978-1-5090-3261-7, pp: 156-161.

Kumar, M.A. and J. Ravindra, 2016. 4x4 MIMO alamouti decoder implementation using VERTEX2. Intl. J. Mag. Eng. Technol. Manage. Res., 3: 67-73.

Lee, J.S. and L.E. Miller, 1998. CDMA Systems Engineering Handbook. Artech House, Norwood, Massachusetts, ISBN:9780890069905, Pages: 1228.

Lipinski, P. and M. Yatsymirskyy, 2008. New approach to orthogonal multiplierless wavelet family synthesis. Proceedings of the 2nd WSEAS International Conference on Mathematics and Computers in Science and Engineering, May 27-30, 2008, WSEAS, Istanbul, Turkey, pp: 163-166.

Mallat, S.G., 1989. Multiresolution approximations and wavelet orthonormal bases of L2(R). Trans. Am. Math. Soc., 315: 69-87.

Mawele, C.C. and R. Pellissier, 2016. A framework for the development of management skills for co-operative development in an agri-business value chain in South Africa. Proceedings of the Portland International Conference on Management of Engineering and Technology (PICMET'16), September 4-8, 2016, IEEE, Honolulu, Hawaii, USA., ISBN:978-1-5090-3595-3, pp: 1429-1441.

Mecklenbrauker, C.F. and M. Rupp, 2004. Generalized alamouti codes for trading quality of service against data rate in MIMO UMTS. EURASIP. J. Appl. Signal Process., 2004: 662-675.

Mehmood, I., M.A. Ashraf and K. Shabir, 2017. Capacity enhancement using adaptive power and sub-carriers allocation under imperfect CSI in MC-CDMA systems. Proceedings of the 14th International Bhurban Conference on Applied Sciences and Technology (IBCAST'17), January 10-14, 2017, IEEE, Islamabad, Pakistan, ISBN:978-1-4673-9074-3, pp: 782-786.

Mehrizi, S. and B. Mahboobi, 2017. Cooperative MIMO relay beamforming in overloaded DS/CDMA multicast networks. IET. Commun., 11: 344-354.

Moskvitch, K., 2017. Securing IoT: In your smart home and your connected enterprise. Eng. Technol., 12: 40-42.

Mota, H.O., F.H. Vasconcelos and R.M.D. Silva, 2005. Real-time wavelet transform algorithms for the processing of continuous streams of data. Proceedings of the IEEE International Workshop on Intelligent Signal Processing, September 1-3, 2005, IEEE, Faro, Portugal, pp: 346-351.

Percival, D.B. and A.T. Walden, 2000. Wavelet Methods for Time Series Analysis. Cambridge University Press, UK., ISBN: 0 5216 4068 7.

Pischella, M. and D.L. Ruyet, 2015. Digital Communications 2Digital Modulations. John Wiley & Sons, New York, USA., ISBN:978-1-84821-846-8, Pages: 299.

Pouryazdan, M., B. Kantarci, T. Soyata, L. Foschini and H. Song, 2017. Quantifying user reputation scores, data trustworthiness and user incentives in mobile crowd-sensing. IEEE. Access, 5: 1382-1397.

Prasad, R., 2004. OFDM for Wireless Communications Systems. Artech House, Norwood, Massachusetts, ISBN:1-58053-796-0, Pages: 275.

Raouf, H., H. Yousef and A. Ghonem, 2014. An analytical comparison between applying FFT and DWT in WiMAX systems. Intl. J. Comput. Sci. Issues, 11: 18-26.

Riju, B., P. Sreevidya and K. Smitha, 2015. Compression and comparison of ECG signals using DWT and DWPT. Indian J. Sci. Technol., 8: 1-5.

Rindani, M.N. and N.M. Rindani, 2015. Performance improvement of 4x4 extended alamouti scheme with implementation of eigen beamforming technique. Intl. J. Comput. Appl., 119: 18-23.

Roy, A.B., D. Dey, B. Mohanty and D. Banerjee, 2012. Comparison of FFT, DCT, DWT, WHT compression techniques on electrocardiogram and photoplethysmography signals. Intl. J. Comput. Appl., 1: 6-11.

Samaraweera, S.A.K.G., N.G.H.P. Gamage, I.G. Gallage, D.D.T.M. Gunathilaka and N. Fernando *et al*., 2017. A trilateral influence model for online shopping. Proceedings of the National Conference on Technology and Management (NCTM'17), January 27, 2017, IEEE, Malabe, Sri Lanka, ISBN:978-1-5090-4730-7, pp: 75-80.

Schulze, H. and C. Luders, 2005. Theory and Applications of OFDM and CDMA: Wideband Wireless Communications. John Wiley & Sons, England, UK., ISBN:9780470850695, Pages: 420.

Sewwandi, D., K. Perera, S. Sandaruwan, O. Lakchani and A. Nugaliyadde *et al*., 2017. Linguistic features based personality recognition using social media data. Proceedings of the National Conference on Technology and Management (NCTM'17), January 27, 2017, IEEE, Malabe, Sri Lanka, ISBN:978-1-5090-4730-7, pp: 63-68.

Shi, J., Z. Song and Q. Ni, 2017b. Distributed resource allocation assisted by intercell interference mitigation in downlink multicell MC DS-CDMA systems. IEEE. Trans. Wirel. Commun., 16: 1250-1266.

Shi, S., D. Jin and G. Tiong-Thye, 2017a. Real-time public mood tracking of Chinese microblog streams with complex event processing. IEEE. Access, 5: 421-431.

Simon, M.K., 2002. Spread Spectrum Communications Handbook. McGraw-Hill, New York, USA., ISBN:9780071382151, Pages: 1229.

Soni, M.A., M.S. Basha and A.C. Tiwari, 2013. Comparative analysis of OFDM under FFT and DWT based image transmission. Intl. J. Innov. Res. Comput. Commun. Eng., 1: 371-378.

Sultana, M., P.P. Paul and M.L. Gavrilova, 2017. Social behavioral information fusion in multimodal biometrics. IEEE. Trans. Syst. Man Cybern. Syst., 99: 1-12.

Verma, G., F.T. Dagefu, B.M. Sadler and P. Spasojevic, 2016. Implications of time/frequency synchronization tradeoff of quasi-synchronous multi-carrier DS-CDMA for robust communications at lower VHF. Proceedings of the IEEE Conference on Military Communications (MILCOM'16), November 1-3, 2016, IEEE, Baltimore, Maryland, USA., ISBN:978-1-5090-3782-7, pp: 694-699.

Wicha, S., T. Photiphun, P. Janjaroenpan, C. Taweesak and I. Chainilwan *et al*., 2017. Proposed of E-Community Supported Agriculture (E-CSA) system to promote local organic products: The empirical study of Chiang Rai province. Proceedings of the International Conference on Digital Arts, Media and Technology (ICDAMT'17), March 1-4, 2017, IEEE, Chiang Mai, Thailand, ISBN:978-1-5090-5211-0, pp: 273-281.

Wickerhauser, M.V., 1994. Adapted Wavelet Analysis from Theory to Software. IEEE Press, New Jersey, USA., ISBN:9781568810416, Pages: 486.

Xu, Z., L. Mei, Z. Lu, C. Hu and X. Luo *et al*., 2017. Multi-modal description of public security events using surveillance and social data. IEEE. Trans. Big Data, 99: 1-12.

Yamakami, T., 2017. A 4-stage mental model of conversion: An approach to capture transition of customer mind. Proceedings of the 19th International Conference on Advanced Communication Technology (ICACT'17), February 19-22, 2017, IEEE, Bongpyeong, South Korea, ISBN:978-1-5090-4892-2, pp: 644-648.

Zhang, B., R. Yong, M. Li, J. Pan and J. Huang, 2017. A hybrid trust evaluation framework for E-commerce in online social network: A factor enrichment perspective. IEEE. Access, 5: 7080-7096.

Zhang, F., J. Feng, J. Bai and Y. Jin, 2015. Energy policy and market space research in electricity of European commission. Proceedings of the 5th International Conference on Electric Utility Deregulation and Restructuring and Power Technologies (DRPT'15), November 26-29, 2015, IEEE, Changsha, China, ISBN:978-1-4673-7106-3, pp: 2591-2595.